# Theoretical Study of Electron−Phonon Relaxation in PbSe and CdSe Quantum Dots: Evidence for Phonon Memory

**ARTICLE** *in* THE JOURNAL OF PHYSICAL CHEMISTRY C · OCTOBER 2011

Impact Factor: 4.77 · DOI: 10.1021/jp206594e



**4 AUTHORS:**

Svetlana Kilina
North Dakota State University
**62** PUBLICATIONS **1,396** CITATIONS
SEE PROFILE

Dmitri Kilin
University of South Dakota
**85** PUBLICATIONS **872** CITATIONS
SEE PROFILE

Victor Prezhdo
University of Rochester
**26** PUBLICATIONS **312** CITATIONS
SEE PROFILE

Oleg Prezhdo
University of Rochester
**306** PUBLICATIONS **6,778** CITATIONS
SEE PROFILE

THE JOURNAL OF PHYSICAL CHEMISTRY C

ARTICLE

pubs.acs.org/JPCC

# Theoretical Study of Electron−Phonon Relaxation in PbSe and CdSe Quantum Dots: Evidence for Phonon Memory

Svetlana V. Kilina,[†] Dmitri S. Kilin,[‡] Victor V. Prezhdo,[§] and Oleg V. Prezhdo*[,∥]

[†]Department of Chemistry and Biochemistry, North Dakota State University, Fargo, North Dakota 58102, United States

[‡]Department of Chemistry, University of South Dakota, 414 East Clark Street, Vermillion, South Dakota 57069, United States

[§]Institute of Chemistry, Jan Kochanowski University, 25-406 Kielce, Poland

[∥]Department of Chemistry, University of Rochester, Rochester, New York 14627, United States

**ABSTRACT:** We have combined analytical theory with *ab initio* nonadiabatic molecular dynamics to study the phonon-induced relaxation of photoexcited charge carriers in PbSe and CdSe semiconductor quantum dots (QDs). Density functional theory calculations show dense distributions of electronic levels near the energy gap, attributed to the reconstruction and lack of absolute symmetry of the QD surface. Most of these states are optically dark, but they do couple to phonons and facilitate charge carrier relaxation. The time-domain simulations show a complex, nonexponential relaxation, in agreement with the observed non-Lorenzian spectral line shapes. The relaxation accelerates at higher photoexcitation energies due to both a higher density of carrier states and a larger nonadiabatic electron−phonon coupling. Over time, carrier relaxation changes from Gaussian to exponential. The Gaussian component is larger in smaller dots; this may be a manifestation of the phonon bottleneck effect. Since Markovian rate models give exponential decay, we suggest that the more complex form of the carrier relaxation, observed in our simulations, can be attributed to phonon memory. The analytic theory developed within the framework of quantized Hamilton dynamics rationalizes this observation. It shows that a detailed description of the phonon modes is more important than a model for the electronic states.

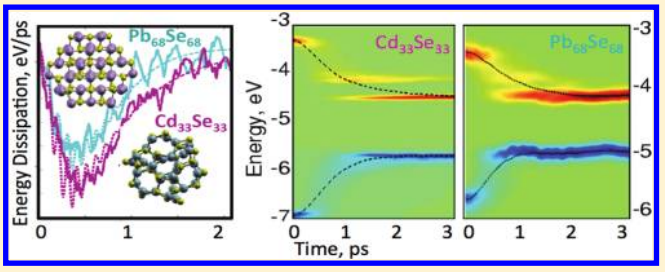


## INTRODUCTION

The dynamics of excited charge carriers, including phonon-induced relaxation of a charge to its ground state, affect many properties of nanoscale devices, such as switching speed, carrier mobility, carrier concentration, and luminescence efficiency. Further, carrier-phonon interactions are enhanced by the strong spatial confinement that occurs in such low-dimensional systems as semiconductor nanocrystals and quantum dots (QDs). In QDs that are smaller than or similar in size to the Bohr exciton radius,[1] carrier confinement dictates size-tunable electronic properties and makes QDs promising materials for various applications. These applications include optoelectronic devices, such as solar cells,[2−5] light-emitting diodes,[6] field-effect transistors,[7] and lasers,[8,9] as well as quantum computers[10,11] and biological imaging probes.[12] In most such applications, both interband and intraband transitions play important roles.

In spite of numerous experimental[2−4,13−16] and theoretical[17−20,22] studies of phonon-mediated relaxations of electrons and holes in QDs, the role that phonons play in intraband transitions remains poorly understood. For example, although relaxation times reported in different QDs range from subpicoseconds to a few picoseconds, which are close to the relaxation time scales in bulk materials, it is still a mystery why the electron−phonon relaxation bottleneck has been observed experimentally only on rare occasions. "Phonon bottleneck" became a historic name for the issue of discrepancy between the theory expectations and experimental observations for phonon-induced relaxation in nanostructures. An expected mismatch of large electronic energy gaps, induced by confinement, with phonon frequencies, should delay dissipative processes in idealized small nanostructures. This effect is not supported by experiment, as it neglects surface states, thermal fluctuations, and other sources of disorder. Agreement is achieved by atomistic description. Even more surprisingly, the experimentally detected carrier relaxation rates in PbSe and CdSe QDs are larger in smaller QDs, where quantum confinement increases the electronic energy spacing.[23−25]

The absence of the phonon bottleneck in QDs has fundamental and practical significance. For example, in a QD gain medium, it is desirable for excited carriers to relax rapidly to their lowest states so that radiative recombination can occur; therefore, the presence of a phonon bottleneck would likely hinder the operation of light-emitting devices. On the contrary, in QD solar materials, carrier multiplication (CM) takes place,[3−5,26] and the existence of a bottleneck would allow CM to compete with carrier relaxation and would increase CM efficiency.

At present, three possible explanations for the absence of the bottleneck have been suggested: carrier relaxation (i) through surface states, (ii) through Auger phenomena,[27] and (iii) through

**Received:** July 12, 2011
**Revised:** September 20, 2011
**Published:** September 22, 2011

many-phonon processes. Carrier trapping in the manifold of surface states can facilitate fast relaxations because high surface-to-volume ratios and imperfections in surface passivation provide impurities and defects in small QDs. In CdSe QDs, it has been shown that electron dynamics strongly depends on surface ligands, while hole relaxation is almost unaffected by passivation.[9,25,28,29] Nevertheless, the role of surface states is not clear because experimental control of QD shapes and surfaces remains a challenge.

Auger electron−hole scattering, as described by Efros et al.,[27] may occur in II−VI and III−V semiconductor QDs when the density of hole states is much larger than the density of electron states. A common example is a CdSe QD; in these QDs, the effective mass of a hole is about six times larger than the electron effective mass.[1] Due to the strong asymmetry between the conduction band (CB) and the valence band (VB), holes relax much faster than electrons.[30] But electrons can lose energy by coupling with dense hole states,[26] providing overall ultrafast relaxation of carriers. When the Auger-type electron−hole energy transfer is intentionally obstructed (electrons are decoupled from holes by spatial separation),[9] relaxation times increase by an order of magnitude, supporting the idea that an Auger-like mechanism opens a new relaxation channel.

However, it is not completely clear how rapid intraband relaxations occur in those materials in which the Auger-like mechanism is inefficient. For instance, semiconductors of the IV−VI group, such as PbSe, have nearly symmetric CBs and VBs and, correspondingly, similar effective masses of electrons and holes.[31] Consequently, Auger relaxation processes are inefficient in these materials, when compared to those in a nanocrystal, such as CdSe, that has asymmetric CBs and VBs. In such cases, relaxation through a multiphonon channel provides a plausible alternative. The possibility of a multiphonon relaxation channel is supported indirectly by the observed temperature-activated behavior of relaxation rates in PbSe QDs.[34] Although relaxation through several phonons is inefficient, because it is a high order process involving a product of multiple electron−phonon coupling matrix elements, the localization of wave functions plus strong nonadiabatic electron−phonon coupling in small QDs make multiphonon processes highly probable.[32−34] When electronic energy gaps exceed single phonon energies, linear electron−phonon relaxation is impossible due to energy conservation, and multiphonon processes can become favorable. Particularly efficient multiphonon relaxation can be supported by those vibrational modes that are able to couple to the electronic degrees of freedom strongly and for extended periods of time. As a result, one may observe rich, non-Markovian electron−phonon dynamics.

Previously, we developed a method based on density functional theory (DFT) for calculating nonadiabatic (NA) electron−phonon coupling and real-time atomistic *ab initio* relaxation dynamics.[35−37] This method applies trajectory surface hopping[38−40] (TSH) within the time-dependent Kohn−Sham (KS) theory.[41,42] TSH is a fully atomistic NA molecular dynamics (NAMD) approach that satisfies detailed balance.[40] It is one of the most common NAMD schemes[43,44] and can be viewed as a quantum master equation for electron dynamics in which state-to-state transition rates depend on time through coupling to explicit phonon dynamics. Although an effective description is available based on *ab initio* MD, there is still the challenge of reducing the computational cost, which would eventually allow us to describe some quantum features of the phonon modes. In the interim, we continue to develop a description of coupled quantized electron-vibrational dynamics that targets the irreversible behavior of the electronic subsystem.

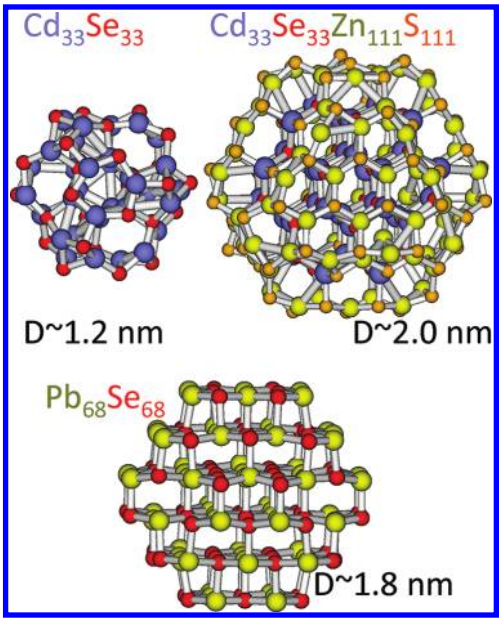


**Figure 1.** Optimized structures of QDs under investigation.

Our methodology has been successfully used to simulate phonon-mediated electron and hole relaxation dynamics in a small (~1 nm in a diameter) PbSe QD.[22,25] It reveals a dense distribution of electronic levels near the energy gap ($E_g$) due to surface reconstructions and the lack of absolute spherical symmetry of the QD. Here, we apply this approach to larger QDs made of different materials, in particular, PbSe and CdSe, that are commonly used in experiments, to investigate the dependence of the carrier relaxation mechanism on material parameters. We focus on the quantum population dynamics of photoexcited electronic states of the QDs. We represent conduction and valence bands as sets of discrete levels arising from an atomistic representation. An initial excitation of a charge carrier is followed by its relaxation from the excited level to the band edge. According to the numerical simulations, only the initially excited and band edge levels experience noticeable population changes; intermediate levels exhibit smalls changes in population and serve an auxuliary role. This allows us to introduce an approximate model, in which only the first and last levels are described explicitly, while the rest effectively couple these two states.

We report results from *ab initio* and analytical studies of NA relaxation dynamics in PbSe and CdSe QDs for various initially excited electron states. Colloidal PbSe and CdSe QDs normally exhibit rock salt and wurzite lattice symmetry. These QDs have drastically different electronic band structures: nearly symmetric CB and VB in PbSe, but strongly asymmetric bands in CdSe.[1,46] Thus, carrier relaxation is expected to be very different in these two materials. Simulations were performed on relatively large semiconductor systems (up to 222 atoms) over a 4 ps duration. The sizes of these systems approach those typical of QDs investigated experimentally. The atomistic representations of these QDs are shown in Figure 1, and the procedures used in the *ab initio* NAMD simulations are described in Appendix I.

The developed analytic model, described in detail in Appendix II, includes an initially excited electron−hole (e-h) pair and an e-h pair at the band gap. The energy difference and wave function overlap for these two e-h pairs are expanded in a power series of atomic

**Table 1. Nonadiabatic Coupling Averaged over Nearest States ($d_{i,i+1}$) and over All States ($d_{total}$) for $Cd_{33}Se_{33}$ and $Pb_{68}Se_{68}$ QDs[a]**

| | | CdSe | | | PbSe | | | |
|---|---|---|---|---|---|---|---|---|
| | | $2E_g$ | $2.5E_g$ | $3E_g$ | $2E_g$ | $2.5E_g$ | $3E_g$ | $4E_g$ |
| electrons | $d_{i,i+1}$ (meV) | 14.6 | 14.8 | 16.7 | 20.4 | 23.6 | 23.8 | 27.8 |
| | $d_{total}$ (meV) | 8.6 | 8.9 | 9.9 | 12.0 | 13.8 | 15.1 | 16.2 |
| | $\kappa$ ($ps^{-1}$) | 0.8 | 1.0 | 1.1 | 0.7 | 1.1 | 1.3 | 1.4 |
| | $\tau$ (ps) | 0.3 | 0.3 | 0.3 | 0.3 | 0.4 | 0.5 | 0.5 |
| holes | $d_{i,i+1}$ (meV) | 22.4 | 22.5 | 22.4 | 30.1 | 31.4 | 32.2 | 33.3 |
| | $d_{total}$ (meV) | 13.2 | 13.3 | 13.2 | 17.7 | 18.4 | 19.0 | 19.5 |
| | $\kappa$ ($ps^{-1}$) | 1.6 | 1.9 | 1.9 | 1.2 | 1.4 | 1.6 | 1.6 |
| | $\tau$ (ps) | 0.4 | 0.5 | 0.5 | 0.25 | 0.3 | 0.3 | 0.2 |

[a] The considered excitation energies are $2E_g$, $2.5E_g$, $3E_g$, and $4E_g$, where $E_g$ is the fundamental energy gap of the QD. Also shown are calculated rates $\kappa$ of electron and hole relaxations for the same excitations. The rates satisfy eq 2, in which $\tau$ is the crossover time that separates the Gaussian and exponential relaxation regimes. Note that $\tau \neq 1/\kappa$. The data show that larger excitation energies correspond to faster electron and hole relaxations in both QDs; this fact is also supported by the increase in the average nonadiabatic coupling with increasing excitation energy.

displacements and velocities. The displacements and velocities were acquired from *ab initio* MD at ambient temperatures. The time evolution of the population transfer between the initially excited and band gap states is formulated in terms of the Heisenberg equations of motion for the conventional spin and phonon operators.[47] In our previous work, the total energy of the electron−phonon system changes with time and approaches equilibrium as described by the reduced density matrix method.[48] In the limit of small Huang−Rhys factors,[49] the total excitation energy of QDs either oscillates or relaxes depending on whether the phonon mode is correlated or thermalized. This time dependence of the excitation energy corresponds quantitatively to the results obtained by TSH averaged over multiple MD trajectories.[22,25]

By combining atomistic simulation with analytic theory, our approach provides novel physical insights into the electron−phonon relaxation dynamics in semiconductor QDs and leads to an explanation for memory effects and phonon coherence. In the next section of this paper we present simulation results for electron and hole relaxations in CdSe and PbSe QDs. Then we present the corresponding theoretical results. Finally, we compare the simulation and theoretical results and discuss the extent to which they reinforce one another. Technical details concerning our numerical and analytical approaches are contained in Appendices I−III.

## RESULTS

**Phonon-Induced Electron and Hole Relaxation.** Electron−phonon relaxation appears in the TSH method as a sequence of NA transitions between electronic energy levels. Each elementary transition reflects the strength of the NA coupling and the detailed balance factor for transitions upward and downward in energy. The NA couplings are obtained along the trajectory based on the adiabatic wave functions for the current moment in time.

Table 1 compares the NA couplings averaged over all electron and hole states involved in the relaxation to those averaged only

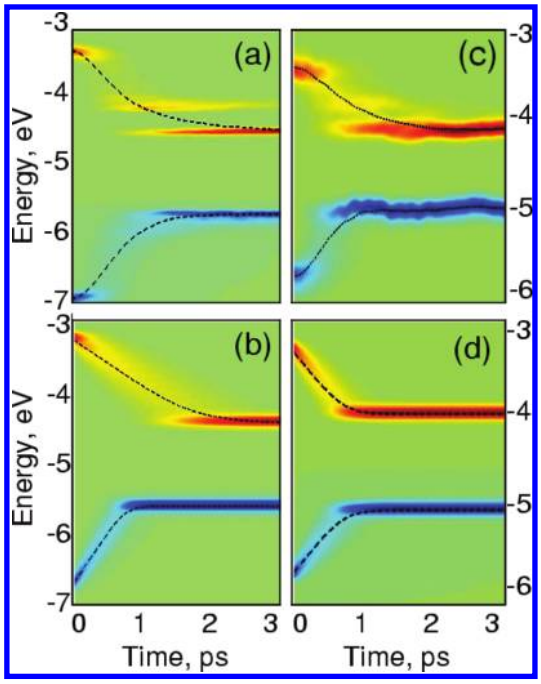


**Figure 2.** Population distributions in energy domain, showing changes in orbital populations relative to equilibrium values. Colors of areas indicate relative changes in the populations: green is the population at equilibrium, red indicates energies having populations above that at equilibrium, and blue indicates energies having populations below that at equilibrium. Intermediate values are represented by a continuous change of colors according to the natural rainbow pattern. Excess (deficient) populations generally develop in conduction (valence) bands. Dashed lines indicate expectation values for energy, calculated in an energy space distribution for conduction and valence bands. Numerical results based on *ab initio* time domain simulations are shown in part a for $Cd_{33}Se_{33}$ and in part c for $Pb_{68}Se_{68}$. These results were obtained from simulations over 3000 fs with ensemble averages formed over 500 replicas. Analytical results based on a Pauli master equation, solved analytically in the Markov approximation, appear in part b for $Cd_{33}Se_{33}$ and in part d for $Pb_{68}Se_{68}$.

over the neighboring states for different excitation energies in the CdSe and PbSe QDs. Because the coupling between nearest states is nearly 1.7 times larger than the coupling averaged over all pairs of states, for both electrons and holes independent of their initial excitation energies, the main contribution to the carrier relaxation should come from neighboring transitions. For both QDs, holes exhibit stronger NA couplings than electrons, rationalizing faster relaxation times for holes. However, this difference is more pronounced for CdSe than for PbSe. Specifically, for excitation energies of $3E_g$, the NA hole coupling in CdSe is 1.8 times larger than the electron coupling, but this ratio is only 1.3 in PbSe QDs. Interestingly, higher excitation energies result in larger average NA couplings and faster relaxations. This result is in qualitative agreement with the experimental data.[24] It can be attributed to a significant increase in the density of states for orbitals that are far from the band gap. A higher state density not only provides more relaxation channels but also favors larger NA coupling. This is because the overlap-type term encountered in the NA coupling is generally larger for states that are close in energy and have similar wave functions. An exception occurs for hole relaxations in the CdSe QD; there the increase in excitation energy only slightly changes the NA coupling and the relaxation

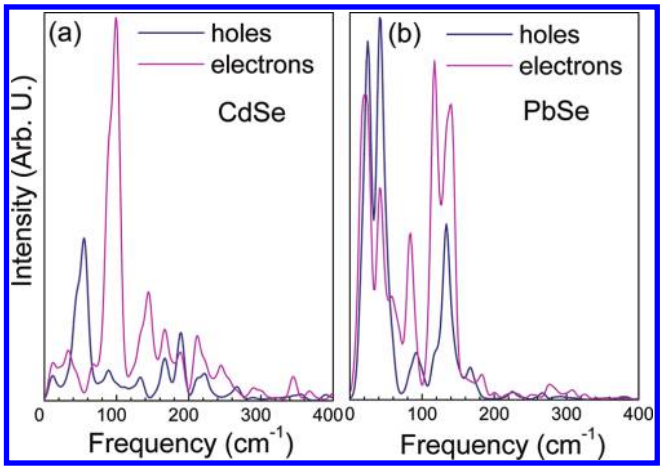


**Figure 3.** Fourier transforms of the energies of initially photoexcited states of holes (blue lines) and electrons (magenta lines) in (a) $Cd_{33}Se_{33}$ and (b) $Pb_{68}Se_{68}$ QDs. In both QDs, each charge carrier interacts with low-frequency phonons; however, electrons couple to slightly faster phonons than do holes. These plots complement a normal-mode analysis: each represents spectra of those phonon modes that are coupled to specific electronic states. A convolution of these plots is proportional to the Stokes shift.

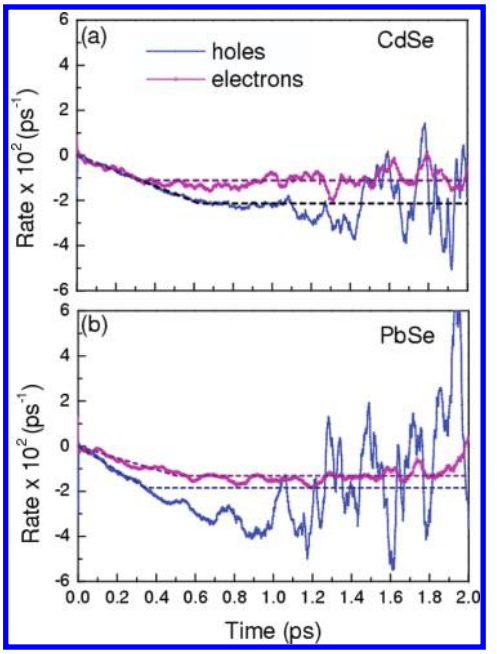


**Figure 4.** Rates of relaxation for electrons (magenta) and holes (blue) from the initial excitation energies of $3E_{gap}$ for (a) $Cd_{33}Se_{33}$ and (b) $Pb_{68}Se_{68}$ QDs. The rates were determined from eq 1. The dashed lines correspond to the fitting function $k(t)$ given in eq 2. The time interval before the crossover time $\tau$ corresponds to Gaussian relaxation with rate constant $K$; after the crossover time the relaxation is exponential, with the same value for rate constant $K$. Values for crossover times are given in Table 1. The equality of the rate constants $K$ in Gaussian and exponential regimes arises from significant electron−phonon coupling (NA coupling). In both QDs, holes relax faster than electrons, (i) because, in these QDs, VBs are more dense than CBs and (ii) because NA coupling between hole states is stronger than that between electronic states. These differences are more pronounced for CdSe, which has a more asymmetric band structure.

rates. This is because hole states are dense even near the band gap due to the asymmetry between the VB and the CB in CdSe.[1]

Results for phonon-mediated electron and hole dynamics for initial excitation energies of $\sim 3E_g$ for both QDs are presented graphically in Figure 2. The figure shows a three-dimensional plot of the product of the density of states (DOS) with the state populations as a function of energy and time. The figure shows that carriers visit multiple states during relaxation, but none of the intermediate states play any special role. Comparing the computed DOS (not shown here) with the population dynamics in Figure 2 shows that, for electrons and holes of both QDs, the initial photoexcitation peak vanishes, only to reappear in the final states. Because of the sparse electron levels near the CB edge in the CdSe QD (due to the smaller size of CdSe), two distinct peaks appear at the final time (3.5 ps): about 95% of the population occupies the LUMO, and about 5% occupies the LUMO+1. In the PbSe QD, the final peak in the CB is broadened over several states from the very edge of the CB, which we previously assigned to $1S_e$. The final hole population for both QDs shows a broad peak centered very close to the HOMO. Thus, for both QDs, carrier relaxation is nearly complete after 3.5 ps.

The average energies of both electrons and holes (dashed lines in Figure 2a and c) plateau after 1.5−2 ps, indicating complete relaxation by that time. Importantly, the average relaxation energy shows very distinct behaviors during the initial and final intervals of time. At the very beginning of the evolution, all charge carriers experience a short period during which transitions with energy loss are about equal to those having energy gains. This short interval is associated with fine quantum effects and corresponds to the development of correlations between charge carriers and phonon subsystems. The electronic transitions couple to a few particular vibrational modes (see Figure 3). These modes stand out in the intensity of electron−phonon coupling and longer dephasing time. The electronic transitions with long-decaying, non-Markovian, autocorrelation function show a richer functional form of dynamics. This regime results in a Gaussian-like shape of energy relaxation. Note that it is possible to distinguish between Gaussian and multiexponential decay by analyzing the first derivative of the data. Gaussian starts with zero slope, and the zero slope is independent of varying temperature. A multiexponential decay has negative slope, which changes with temperature. Later, at times larger than the typical phonon-correlation time, energy relaxation develops into an exponential decay with rates for electrons differing from those for holes. Overall, for both QDs, the relaxations of electron and hole energies in Figure 2 have a nonexponential character, which agrees with the strongly non-Lorentzian line shapes observed experimentally.[17]

Probability density distributions for electron and hole transitions are functions of the transition energy. Transitions occur both up and down in energy; however, downward transitions dominate, as required by detailed balance. The overall energy flow from charged particles to phonons is responsible for the relaxation of the initial photoexcitation. The more likely transitions involve small amounts of energy that exceed the energy of a single phonon, which is around 100 or 200 $cm^{-1}$ (0.012 or 0.025 eV), as shown in Figure 3. However, up to 0.3−0.6 eV of electron energy can occasionally be lost in a single event. This usually happens during electron transitions and is most pronounced in small PbSe QDs[22] and in CdSe QDs. The presence of transitions with energies at least ten times larger than that of the most active phonons supports the idea of a multiphonon relaxation channel in QDs. Thus, we conclude that electron−phonon relaxations in QDs, and

specifically in a small CdSe dot, can occur primarily via a multiphonon mechanism.[16,34]

**Simulated Rates of Relaxation.** To quantitatively estimate relaxation rates in CdSe and PbSe, as well as compare Gaussian and exponential regimes of carrier relaxation, scaled relaxation rates $\kappa(t)$ were determined from time derivatives of average carrier energies by

$$\kappa(t) = \frac{\mathrm{d}\langle E_c\rangle(t)/\mathrm{d}t}{(\langle E_c\rangle(t) - \langle E_f\rangle)} \quad (1)$$

Here, $\langle E_c\rangle(t)$ is the average electron (or hole) relaxation energy at time $t$ and $E_f$ is the average energy of a carrier at the end of the time interval. Typically, $\langle E_f\rangle$ is close to $E_{\mathrm{LUMO}}$ or $E_{\mathrm{HOMO}}$ for electrons or holes, respectively. Since the energies of the band gaps and electronic transitions differ for different QDs, eq 1 allows consistent comparisons of relaxation rates $\kappa$ for QDs with various electronic structures, independent of the absolute values of the energies.

Figure 4 illustrates the dependence of relaxation rate $\kappa$ on time for both QDs initially photoexcited to the energy triple of the band gap of the QD. The overall shape of $\kappa(t)$ in Figure 4 assumes the carrier relaxation rate decays nearly linearly at times smaller than the charge carrier−phonon correlation time $\tau$ (the crossover time). After the crossover time, the average rate does not change, but the instantaneous rate fluctuates around some constant. Thus, a simple fitting of the rates takes the following form:

$$\kappa(t) = \begin{cases} -Kt, & t < \tau \\ -K, & t > \tau \end{cases} \quad (2)$$

The time interval before the crossover time corresponds to Gaussian relaxation with the rate constant $K$, while after the crossover time the relaxation is exponential with the same rate constant $K$. The equality of the rate constants in the Gaussian and exponentional regimes occurs because of significant NA electron−phonon coupling (several meV) in both QDs. The fitting parameters, based on eq 2, for rates calculated for different initial excitation energies are given in Table 1.

The TSH approach provides the dynamics of carrier relaxation in QDs through the solution of the following equations for the Kohn−Sham orbital populations,

$$\mathrm{d}P_{km} = \frac{b_{km}}{a_{km}}\,\mathrm{d}t \quad (3)$$

where

$$b_{km} = -2\mathrm{Re}(a^*_{km}\mathbf{d}_{km}\cdot\dot{\mathbf{R}}), \quad a_{km} = c_k c^*_m \quad (4)$$

Here, $\mathrm{d}P_{km}$ is the probability of a hop occurring between states $k$ and $m$ within time interval $\mathrm{d}t$, $(\mathbf{d}_{km}\cdot\dot{\mathbf{R}})$ is the NA coupling, $\dot{\mathbf{R}}$ is the time-derivative of ionic positions, while $c_k$ and $c_m$ are wave function coefficients. The dot product of gradient matrix element $\mathbf{d}_{km}$ and the nuclear velocity $\dot{\mathbf{R}}$ is calculated as a single number, at each time step for each pair of electronic states $k$ and $m$. The procedure was discussed in more detail in our earlier works.[22,25] The system of ordinary differential eqs 3 has solutions in the form of linear combinations of exponentials; but solutions occur only for constant and real coefficients, i.e., in the Markov limit.[50] The nonexponential profile (the Gaussian form) of the population decay present in the current simulation is due to the explicit time dependence of the relaxation rates in eq 3, providing a slow damping of the autocorrelation function, as was shown elsewhere.[20] The TSH method correctly represents the vanishing time derivative of the quantum-mechanical transition probability at zero time, which is manifested in the quantum-Zeno effect.[21,51] This gives the Gaussian relaxation component at early times—prior to the crossover time $\tau$—before a system enters the **single- or multi**-exponential (Markov) regime of relaxation.

The Gaussian regime is associated with phonon coherency in QDs. Initially, the electronic system is prepared in a pure state in which electron−phonon correlations are maximal. Due to the statistical average, the electronic system is coupled to an ensemble of ionic subsystem replicas with a distribution of positions and momenta over a phase space. During a relatively short time interval, all replicas included in the ensemble move coherently in the same direction, preserving the phase relationship; the center of the replica distribution follows this motion as well. Later, for times after the crossover time $\tau$, the differences in frequencies and initial phases create a destructive interference between replicas, so the center of their distribution gradually stops moving.

This destructive interference (dephasing) depends on the individual features of the phonon subsystem. Thus, the higher the *phonon* density of states, the faster dephasing occurs. Because the phonon density of states scales linearly with QD size, the crossover time $\tau$ is shorter for larger dots and longer for smaller dots. Accordingly, the phonon bottleneck effect can play two roles. First, it can change the rate of relaxation, making it faster or slower; second, it can change the functional dependence of relaxation dynamics. In our studies we do not see the first, but we do see the second. Specifically, in the regime $t < \tau$, eq 3 demonstrates memory effects, particularly in small QDs, and carrier relaxation is nonexponential. However, in the regime $t > \tau$, eq 3 demonstrates no memory effects, and carrier relaxation is exponential. We observe that larger QDs exhibit memory effects over a shorter time range. For instance, for the larger $Pb_{68}Se_{68}$ QD, the calculated crossover times were $\tau = 0.3$ for holes and $\tau = 0.5$ for electrons, but for the smaller $Pb_{16}Se_{16}$ QDs, they were $\tau = 0.4$ ps for holes and $\tau = 0.6$ ps for electrons. Although we find that dephasing times are shorter than the estimated crossover times in QDs, note that our approach allows only a rough evaluation of $\tau$. For more accurate calculations of phonon-induced dephasing times in QDs, time-dependent Kohn−Sham (TDKS) molecular dynamics coupled to the framework of the optical response function within a semiclassical formalism have been applied to $Pb_{16}Se_{16}$ and $Pb_{68}Se_{68}$ QDs. The results were predicted dephasing times of around 10 fs.[20]

For all QD photoexcitation energies we studied, relaxation occurs between 1.4 and 0.5 ps, clearly demonstrating the absence of the bottleneck even in such small clusters. Still, even the fastest relaxation is at least two times slower than carrier multiplication (CM) times, which have an observed upper bound of 250 fs.[4,5,14,26] Generally, both electron and hole relaxation rates speed up with increases in excitation energy. However, hole relaxations in CdSe exhibit almost no rate dependence on the initial excitation due to the very dense VB in this QD. In both QDs, holes relax faster than electrons, which is attributed to a more dense VB compared to the CB, as well as to stronger NA coupling between hole states than electronic states. However, this difference is more sharply pronounced (holes relax almost twice as fast as electrons) for CdSe, which has the more asymmetric band structure. For $2.5E_g$ and $3E_g$ excitations, both electrons and holes in the CdSe QD relax slightly faster than carriers in the PbSe QD. This is in agreement with experimental observations.[34] However, in real CdSe this trend is enhanced by efficient Auger recombination processes, which take

Table 2. Parameters for the Analytical Model Developed in Appendix II [a]

| model | $\hbar\omega_{vib}$ (meV) | $k_BT$ (meV) | $\mu$ (meV) | $g$ (meV) |
|---|---|---|---|---|
| $Pb_{16}Se_{16}$ | 8.40 | 20.34 | 9.77 | 7.51 |
| $Cd_{33}Se_{33}$ | 20.06 | 21.96 | 12.23 | 13.80 |
| $Pb_{68}Se_{68}$ | 20.06 | 24.67 | 9.96 | 13.53 |

[a] The four-parameter fit reproduces the relaxation dynamics. The parameter values are found within reasonable ranges, as justified in the last paragraph of Appendix III.

place through electron coupling with very dense hole states. In contrast, in real PbSe the trend is depressed by the nearly symmetric band structure.

## RESULTS FROM THEORY AND ANALYSIS OF SOLUTION

To describe the relaxational dynamics of semiconductor quantum dots, we express an average energy of excitation by

$$E(t) = E_f + \Delta E[\langle S_z\rangle(t) - \langle S_z\rangle(\infty)] \qquad \Delta E = E_i - E_f \tag{5}$$

Here, $E_i$ and $E_f$ are exciton energies at the initial and final instants of the TDDFT simulation, respectively, $\Delta E = E_i - E_f$ is the energy lost by an e-h pair in the course of relaxation, and $\langle S_z\rangle(t)$ is taken from the model described in Appendix II. Table 2 provides effective $\langle S_z\rangle(t)$ model parameters for describing carrier relaxation in CdSe and PbSe quantum dots of three sizes.

According to our model, the transition from the dynamical regime to the relaxational regime occurs because the energy from the primary vibrational modes is dissipated to the bath. Initially, only one or, at most, a few primary active phonon modes are excited to coherent states; but later, they exchange phase and energy with the rest of the vibrational modes and equilibrate to the thermal state. One can analyze this as follows: At time $t = 0+$, right after excitation by a short pulse, the phonon modes and electronic subsystems are assumed to be decoupled from each other. A short time after the excitaton, correlations between vibrational modes in a region of specific frequency begin to appear. These modes affect electronic evolution in a dynamic way. As time passes, vibrational modes acquire different phases due to differences in their frequencies. So-called dephasing occurs and, at this stage, the motion of vibrational modes is considered to be quasichaotic with respect to its influence on electronic evolution. Here, we estimate this process as a gradual decrement in the correlation $\langle S_z\gamma\rangle$ between the electronic population $\langle S_z\rangle$ and the total number of quanta in the interacting subspace of the electron−phonon manifold $\langle\gamma\rangle$. As a very rough approximation we assume $\langle S_z\gamma\rangle \simeq \langle S_z\rangle\langle\gamma\rangle$. In numerical simulations the corresponding transition from correlated to quasichaotic behavior of vibrational modes can be followed by observing the autocorrelation function of relevant electronic terms whose energy performs quasiperiodic (almost chaotic) motion due to the molecular dynamcs of atoms.[20] The truncated chain of equations of motion for the inversion term $\langle S_z\rangle$ was acquired from the literature.[47] The overall energy $\langle\gamma\rangle$ is composed of electronic and vibrational contributions and is presented in more detail in Appendix II. The equations of motion and solutions for vibrational contributions were also acquired from earlier work.[48]

Note that this mechanism cannot provide an inversion larger than the initial one. We focus on four qualitatively different regimes of coupled electron−phonon dynamics. A qualitative summary of possible regimes of evolution is presented in Table 3: a coherent regime of evolution (i−ii) sooner or later becames a thermalized one (iii−iv).

Table 3. Qualitative Description of Regimes of System Behavior According to the Analytical Solution of the Model in Appendix II

| no. | state of vib. mode | phonon−phonon coupling | temp |
|---|---|---|---|
| i | coherent | small | 0 |
| ii | coherent | large | 0 |
| iii | thermalized | any | low |
| iv | thermalized | any | high |

Also note that the thermalized state of the system $\langle\gamma\rangle$ is a function of temperature. In fact, an interesting dependence was observed for the temperature dependence of the final population of the system,

$$\langle S_z\rangle(\infty) = \frac{(\omega_{vib} - \Omega)^2}{(\omega_{vib} - \Omega)^2 + g^2\langle\gamma\rangle(T)} \tag{6}$$

Therefore, for larger temperatures $T$ and larger $\langle\gamma\rangle$, the inversion becomes smaller and the populations of the initial (donor) and final (acceptor) states approach each other.

## COMPARISON OF DFT AND ANALYTICAL RESULTS

To compare our analytical results with our simulation results, we first return to Figure 2. In that figure, panels a and c contain results from first-principle time-domain simulations of electronic dynamics (DFT). Panels b and d contain results calculated from Pauli master equations (PMEs) using the constant coefficients given in Appendix III. In the PbSe model, electrons and holes relax at similar rates, but in the CdSe model, holes relax faster. An intraband relaxation occurs through a quasi-continuum of intermediate states; therefore, only initially populated KSOs and final states (HOMO/LUMO) exhibit significant population changes. When the initial and final states belong to the same band, populations of intermediate states involved in the relaxation are close to zero.

Figure 2 allows us to compare results from *ab initio* simulations and PME calculations for the time evolution of the expectation values of the energy for conduction $\langle E\rangle^{CB}(t)$ and valence $\langle E\rangle^{VB}(t)$ bands. The *ab initio* results show that, at the initial time $t \rightarrow +0$, the average energy of a carrier first does not change $\langle E\rangle(t) \simeq$ const, then it assumes a Gaussian form, and finally it evolves to an exponential. However, the results obtained from the Pauli master equation with time-independent coefficients provide only an exponential relaxation for $\langle E\rangle(t)$.

Figure 5 presents the main results: the time dependence of the average excitation energy, which is the difference between hole and electron energies,

$$\langle E\rangle^{EX}(t) = \langle E\rangle^{CB}(t) - \langle E\rangle^{VB}(t) \tag{7}$$

These results were obtained by three methods: *ab initio*, PME, and quantized electron−phonon dynamics. Since the three curves are very similar for each QD in Figure 5a, we show in Figure 5b time derivatives of the average excitation energy, to amplify small features.

In the electron−phonon dynamics calculated from first principles, the average energy of an excitation does not initially

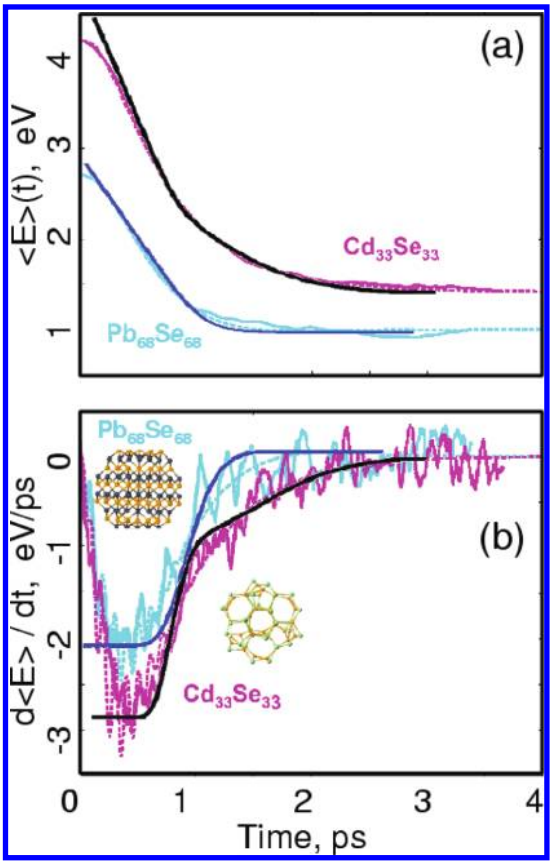


**Figure 5.** Excitation energy dynamics (a) and energy relaxation rates (b) in $Cd_{33}Se_{33}$ and $Pb_{68}Se_{68}$ QDs. Magenta (cyan) solid lines are *ab initio* results for CdSe (PbSe). Magenta (cyan) dashed lines are analytical results from eq 5 for CdSe (PbSe). Black (blue) solid lines are results from a Pauli master equation based on refs 13 and 14; at small times these two agree with ref 15. The insets in part b show geometries of $Cd_{33}Se_{33}$ and $Pb_{68}Se_{68}$ quantum dots. A tangent line to $\langle E\rangle(t)$ reads $\langle E\rangle(t)E_0 - \Gamma\varepsilon t$ and can be extrapolated until it intersects with line $\langle E\rangle(\infty)$. The specific time of this intersect depends on the slope of $\langle E\rangle(t)|_{t\to 0}$ and equals $\tilde{t} = \langle E\rangle(0)/\Gamma\varepsilon = (N\varepsilon)/(\Gamma\varepsilon)$. The larger the number of orbitals, the better the linear approximation for $\langle E\rangle(t)$; the estimation of the relaxation times is proportional to the number of orbitals; and the relaxation rate is an inverse of the number of orbitals $\tilde{t}^{-1} = \Gamma/N$. By the same $\Gamma$, the quantum dot with more orbitals involved in a photoexcitation experiences slower relaxation, in contradiction with the phonon bottleneck hypothesis.

change, then it has a Gaussian character, and then it relaxes exponentially. This dynamical pattern must also be followed by the average energies of electrons and holes because the average total excitation energy is a linear combination of the separate electron and hole energies. Results obtained by integrating the analytical model of quantized electron−phonon dynamics follow the same dynamical pattern as the results from the time-domain DFT calculations: both methods yield results that start with zero rates of relaxation, reach maxima, and then decrease. However, results obtained from the Pauli master equation with time-independent coefficients provide only an exponential relaxation; that is, the PME results start with a constant rate of relaxation and subsequently decrease. Interestingly, the analytical model reproduces tiny oscillations in the relaxation rate (see Figure 5b) that originate from explicit tracking of the active vibrational mode.

## CONCLUSIONS

We have used three approaches to study phonon-induced carrier relaxations in quantum dots: time-domain first-principle simulations, solutions to a Pauli master equation with constant coefficients, and analytical solutions of a simplified model. Our results show that the dense distribution of electronic levels near the energy gap can be attributed to surface reconstructions and the lack of absolute spherical symmetry of the QD surface. The ratio of the number of such states to the number of core states is higher for smaller dots than for larger ones. Most of these states are optically dark and are not activated in absorption spectra, but they do couple to phonons and facilitate carrier relaxation processes. Spacings between state energies were found to nearly match phonon frequencies, except at a few levels near the energy gap. While the calculated optical absorption spectra of QDs do show discrete bands, as observed experimentally, phonons of various symmetries couple most to nearly dark states; these dark states originate from surface reconstructions, and the resultant couplings create an auxiliary pathway for carrier relaxation.

Our simulations demonstrate that the phonon bottleneck is avoided through two relaxation pathways: surface states and multiphonon processes. The latter are enhanced in smaller dots. For both CdSe and PbSe QDs, our results reveal a stronger coupling of carriers to acoustic phonons than to optical ones. The coupling to low-frequency acoustic phonons rationalizes the ultrafast dephasing times and large homogeneous line widths of the optical transitions detected experimentally. Our results also address these issues: (a) how carrier relaxation rates are affected by the QD material, (b) how relaxation rates are affected by the incident photon frequency, and (c) whether there is evidence for phonon memory effects.

**a. Effects of QD Material on Carrier Relaxation.** PbSe and CdSe QDs, which exhibit rock salt and wurzite lattice symmetry, have qualitatively different electronic band structures: nearly symmetric CB and VB in PbSe but strongly asymmetric ones in CdSe QDs. Our simulations support the nearly symmetric structure of the DOS in PbSe dots and an asymmetric DOS in CdSe QDs that is skewed toward the valence band. Since CB levels in CdSe QDs are more dense than VB levels, hole relaxation occurs faster in CdSe. However, in both QDs, electron relaxations have almost the same rates and demonstrate multiphonon characteristics.

**b. Effects of Incident Phonon Frequency on Carrier Relaxation.** For both materials, we find that the higher the energy of the initial excitation, the faster electron relaxation occurs. This is supported by a positive correlation between the average nonadiabatic coupling and the excitation energy and by the fact that the density of levels is much higher for carrier states far from the gap than for carrier states close to the gap.

**c. Evidence for Phonon Memory Effect.** Our *ab initio* simulations show that carrier relaxations change, over time, from a Gaussian-like form to an exponential form. The duration of the Gaussian regime is expected to change inversely with the dot size; this may be a partial implementation of the phonon bottleneck effect. Since simple rate models in the Markovian limit typically generate exponential damping, we suggest that the more complex form of the carrier relaxation, observed in our simulations, can be attributed to phonon coherence. We also suggest that further focus on this issue may reveal important non-Markovian memory effects.

To analyze the hypothesis of a phonon memory effect in quantum dots, we have applied two theoretical models. We

focused on the time evolution of the average energy of an electron−hole excitation and population inversion. These were derived within a QHD framework for coupled electron−phonon evolution and depend on four parameters: vibrational frequency, temperature of phonon bath, vibrational damping, and an average electronic NA coupling.

Our theoretical modeling supports the specific form of relaxation found in the simulations: carriers initially relax as a Gaussian and then exponentially. These forms occur sequentially, not simultaneously. Thus, our theoretical and *ab initio* simulation results all support the hypothesis of a phonon memory effect. In addition, both the *ab initio* and QHD approaches provide a qualitative difference between the dynamics in CdSe and PbSe QDs: the CdSe model exhibits a longer period of Gaussian behavior compared to that seen in the PbSe model. Finally, in the QHD method, the rate of relaxation depends on phonon−phonon interactions as described here by a vibrational damping parameter.

We conclude that the important features of carrier relaxation require a more or less explicit description of phonon modes. In fact, a description of phonon modes is shown to be more important than a detailed description of electronic states: the specifics of electron relaxation depend drastically on phonon−phonon interactions and on a coherence time for phonons. More generally, details from our studies advance our understanding of QD properties, reconcile the seemingly contradictory observations of wide optical line spacing and lack of a phonon bottleneck to the relaxation, and rationalize why highly efficient carrier multiplication is possible in PbSe and CdSe nanocrystals despite the absence of the phonon bottleneck.

## APPENDIX

**Appendix I. Numerical Approaches.** The models used in this study of PbSe and CdSe QDs are shown in Figure 1. The initial geometries of the clusters were generated on the basis of the bulk structures of CdSe and PbSe. Then, the QDs were fully relaxed and optimized at zero temperature. To keep the simulations feasible, surface ligands were not included. In the case of PbSe, this is justified because surface effects in PbSe QDs are known to be small relative to those in other types of semiconductors.[31] In the case of CdSe QDs, we checked the effect of a surface reconstruction on the electronic structure (specifically, on near-gap levels): the core-shell cluster $Cd_{33}Se_{33}/Zn_{111}S_{111}$ was used, and the electronic structures of pure CdSe and the core-shell CdSe/ZnS were compared.

The optimized configurations for $Cd_{33}Se_{33}$ and $Pb_{68}Se_{68}$ were brought to 300 K using molecular dynamics with repeated velocity rescaling. A microcanonical trajectory was generated for each cluster using the Verlet algorithm with Hellmann−Feynman forces. The time step was 2 fs for PbSe and 3 fs for CdSe, producing 4 and 3.6 ps trajectories, respectively. The structures shown in Figure 1 were chosen randomly from these trajectories, indicating that the clusters preserve their bulk topology during the simulations. The classical treatment of ion motion is justified at room temperature because the frequencies of the available vibrational modes are on the order of or less than $kT/p$.

Geometry optimization and adiabatic molecular dynamics were both performed by plane wave DFT simulations implemented in the VASP[52,53] code, which is particularly efficient for semiconductor crystals and surfaces. The core electrons were simulated using the ultrasoft Vanderbilt pseudopotentials,[54] while all valence electrons were treated explicitly. The generalized gradient functional due to Perdew and Wang (PW91)[55] was used to account for electron exchange and correlation effects. The simulations were performed using plane wave basis sets with over 106 plane waves corresponding to an energy cutoff of 396.0 eV, which is large enough for convergence of electronic energies in these systems.

**Appendix II. Theoretical Model of Electron−Phonon Interactions.** The model developed here is based on the view that energy transfers are modulated by a Hamiltonian that contains (i) electronic degrees of freedom, (ii) a primary nuclear "active" mode that is involved in electron−phonon coupling processes, and (iii) the remaining phonon modes, which affect only the primary mode and, therefore, affect electron transfer/relaxation processes only in an indirect way.[56] This approach rests on extracting such parameters as frequencies, energies, and displacements from *ab initio* calculations. In a ground state, relaxed geometry, all electronic eigenstates are orthogonal to each other; however, slight changes in atomic positions break this orthogonality and couple electronic states. We describe this by the following Hamiltonian

$$H = H_{\text{el-ph}} + H_{\text{bath}} + V$$

Here $H_{\text{el-ph}}$ includes electronic degrees of freedom, the primary active phonon mode, and interactions between them. The term $H_{\text{bath}} + V$ contains the other phonon modes and the interaction between those modes and the primary active phonon mode. The bilinear coupling between the active mode and the rest of the bath is written as

$$V = \Sigma_\xi \kappa_\xi (a + a^+)(b_\xi + b_\xi^+)$$

To reduce the computational effort, we apply a reduced description, which we refer to as QHD. Since our primary goal is the population dynamics of electronic states, we build an operator that describes this population inversion and that tracks its expectation value; the approach is based on the Heisenberg equation of motion for this operator as well as equations for any operators appearing therein.

For two electonic levels and one active mode, $H_{\text{el-ph}}$ takes the form[47]

$$H_{\text{el-ph}} = \hbar\omega(a^+a + 1/2) + \hbar\Omega S_z + g\hat{\alpha}$$

where $g$ is the nonadiabatic coupling and the time evolution of the number of quanta in the active mode can be expressed as a function of mode frequency $\omega$, coupling $\kappa_\xi$, dissipations $\mu = \kappa_\xi^2 j(\omega)$, normalized frequency $\tilde{\omega}^2 = \omega^2 + \mu^2$, and thermal Bose−Einstein distribution $n = n(\omega,T)$

$$\langle a^+a\rangle = n + \exp\{-2\mu t\}\left[|\alpha_0|^2 - n\left(\frac{\omega}{\tilde{\omega}}\right)^2 + 2|\alpha_0|^2\frac{\mu}{\tilde{\omega}}\sin 2\tilde{\omega}t + n\left(\frac{\mu}{\tilde{\omega}}\right)^2\cos 2\tilde{\omega}t\right] \quad (8)$$

Note that here the oscillatory part vanishes at small couplings $\kappa_\xi$ and dissipations $\mu$. Here the auxiliary operators include electron−phonon interactions $\alpha,\beta = a^+S_- \pm aS_+$ and the

operator for the number of quanta $\gamma = a^+a + {}^1/_2 + S_z$. The relevant system of Heisenberg equations of motion reads

$$\begin{aligned} i\frac{\mathrm{d}}{\mathrm{d}t}\langle\alpha\rangle &= -\delta\langle\beta\rangle \\ i\frac{\mathrm{d}}{\mathrm{d}t}\langle\beta\rangle &= -\delta\langle\alpha\rangle - 2i\mu\langle\beta\rangle + g\langle\gamma S_z\rangle \\ i\frac{\mathrm{d}}{\mathrm{d}t}\langle S_z\rangle &= g\langle\beta\rangle \end{aligned} \tag{9}$$

This system of equations is truncated by the approximation $\langle\gamma S_z\rangle \approx \langle\gamma\rangle\langle S_z\rangle$.[57] In contrast to other work[47] where $\mathrm{d}\gamma/\mathrm{d}t \equiv 0$ and $\langle\gamma\rangle = \langle\gamma\rangle(0)$, we allow fluctuations in $\gamma$. In the presence of the bath, the number of quanta $\langle\gamma\rangle$ oscillates slightly around its thermal equilibrium value and it enters eq 9 adiabatically, as a parameter. For the simple choice of initial conditions $\langle\alpha\rangle(0) = 0$, $\langle\beta\rangle(0) = 0$, and $\langle S_z\rangle(0) = \langle S_z\rangle_0$, eq 9 provides different solutions depending on the value of the parameter $\lambda$,

$$\lambda(t) = 0, \quad \pm\sqrt{\mu^2 - \Delta^2(t)}$$

For $\Delta < \mu$, $\lambda$ has real values, while, for $\Delta > \mu$, $\lambda$ takes imaginary values. Here, $\Delta^2(t) = \delta^2 + g^2\langle\gamma\rangle(t)$ mimics the modulation of electronic energies by phonon motion.

The solution to eq 9 is

$$\langle S_z\rangle(t) = \langle S_z\rangle(0)\left(\frac{\delta^2}{\omega^2} + \exp(-\mu t)Z(t)\right) \tag{10}$$

$$Z(t) = \frac{g^2\langle\gamma\rangle(t)}{\Delta^2(t)}\left[\cosh(\lambda(t)t) + \frac{\mu}{\lambda}\sinh(\lambda(t)t)\right] \tag{11}$$

$$\langle\gamma\rangle(t) = \langle S_z\rangle(0) + \underbrace{\frac{1}{2} + \langle a^+a\rangle(t)}_{\text{vib.energy}} \tag{12}$$

As it is, this model explicitly describes two levels, e.g., a pair of individual states of neighboring energy in a quantum dot. However, it seems possible that this solution for two levels could be extrapolated to describe electronic dynamics in the excitonic band of a semiconductor quantum dot. To do so, we use an effective coupling parameter $\bar{g}$ and an effective detuning parameter such that this model approximately describes the relaxation of the continuous band. As shown in Appendix III, this approach describes the coupling between first and last states when those states are, in reality, coupled through a chain of auxiliary states. Here, effective detuning corresponds to the minimal detuning between neighboring levels in such a chain.

Technically, the solution provides reasonable behavior: as soon as thermal equilibrium is established, the upper level is drained and the lower is overpopulated. At that point, the upper level can be excluded from consideration and the new lower level is included. This approximate description mimics the paradigm of the surface-hopping approach, in which, during an individual run, the electronic population occupies only one state (excluding superpositions). To fit the relaxational dynamics of semiconductor quantum dots, we use the representation in eq 5 for the average energy of excitation.

**Appendix III. Justification of the Theoretical Model: Representation of Continuous Bands by Two-Level Systems.** In this Appendix we give arguments to support the use of a two-level model to mimic continuous bands in semiconductor quantum dots. We also present background for the parameter conversion convention. We seek to establish a well-defined correspondence between parameters of a two-level system and an N-level band of a semiconductor QD such that we obtain the same relaxation rate for both models.

It is known that the density of states scales as $\mathrm{d}N/\mathrm{d}E \approx E^{-1/2}$ in one dimension, as $E^0$ in two dimensions, and as $E^{1/2}$ in three dimensions. Therefore, an equidistant model is most suited for 2D systems, e.g., thin films. However, for a high density of states and in the vicinity of a given energy $E_0$, one can assume $\mathrm{d}N/\mathrm{d}E \approx \mathrm{d}N/\mathrm{d}E(E_0) + O^2 \approx$ const.

Consider a simple model representing the conducting band of a quantum dot. The model consists of an infinite number of levels $i = 0, 1, ..., N, ...$, in which neighboring levels are separated by an energy difference $\varepsilon$. For any pair of levels, transitions between the two result from nonadiabatic couplings induced by thermal motion of the same phonon bath. Since transitions between neighbors dominate any other transitions, we consider only transitions betwen neighbors. Further, only the energy difference $\varepsilon$ between neighbors affects relaxation rate, Boltzmann factors, and any other kinetic variables.

The calculation of an observable, such as an expectation value of energy, is based on an average over the conduction or valence band. Here we focus on the long-time scale where coherent effects are negligible. For simplicity we suppose that the low-temperature limit, e.g., transitions down in energy, dominates thermal activation processes. This kinetic model is well suited to the long-time limit, where all dynamical effects have dephased.[58] The dynamics of such systems typically have simple solutions for times larger than the inverse of the dephasing time $\gamma^{-1}$. In this limit, the Laplace transform of the equation of motion for the density matrix in the basis of adiabatic states simplifies in that the factor $(i\varepsilon/\hbar + \gamma + s)^{-1} \approx (i\varepsilon/\hbar + \gamma) + O(s)$ loses the Laplace-transform variable. This approximation allows us to substitute expressions for nondiagonal elements of the density matrix EOM into expressions for the diagonal ones, eliminating the former from explicit consideration.[58−60] As a result, the density matrix equation takes the following form, involving gain and loss terms,

$$\dot{\sigma_{jj}} = \sum_k d_{jk}\sigma_{kk} - \sum_k d_{kj}\sigma_{jj}$$
$$\text{gain} \qquad\qquad \text{loss}$$

Recasting this equation for occupations of the levels $P_i = \sigma_{ii}$, we obtain this Pauli master equation,[61]

$$\frac{\mathrm{d}}{\mathrm{d}t}P_j = \sum_k d_{jk}P_k - \left(\sum_k d_{kj}\right)P_j$$

Here the $d_{jk}$ are transition probabilities for nearest neighbors,

$$d_{jk} = \bar{d}\delta_{k,j+1} + \bar{\bar{d}}\delta_{k,j-1}$$

and the transition probabilities $d_{ij}$ obey a detailed balance relation,

$$d_{jk}/d_{kj} = \exp\{-(\varepsilon_j - \varepsilon_k)/k_BT\}$$

Invoking the approximations stated above, we keep only transitions downward with the same rates, so as $k_BT \to 0$ with $\Sigma d_{kj} = \Gamma$, we have

$$\dot{P}_i = -\Gamma P_i + \Gamma P_{i+1} \tag{13}$$

Here an initial condition corresponds to the instantaneous excitation to an orbital $N$ of a given band $P_i(0) = \delta_{iN}$. The simple rate equation, eq 13, retains this form for each $0 < i < N$. For the initially excited state $N$, eq 13 takes the form $\dot{P}_N = -\Gamma P_N$,

while at the band edge $i = 0$, it takes the form $\dot{P}_0 = \Gamma P_1$. All remaining populations, $P_i$, for $i > N$ remain at zero for all times,

$$\frac{d}{dt}P_i(0) = 0, \quad P_i(t) = P_i(0) = 0$$

The recursive solutions to this set of rate equations, starting from higher index levels and proceeding down to the band edge, are as follows:

$$P_{i>N} = 0$$
$$P_N = e^{-\Gamma t}$$
$$P_{N-1} = t\Gamma e^{-t\Gamma}$$
$$\vdots$$
$$P_1 = \frac{1}{(N-1)!}(\Gamma t)^{N-1} \quad \exp\{-\Gamma t\}$$
$$P_0 = 1 - e^{-t\Gamma}\left\{1 + \Gamma t + \frac{1}{2}(\Gamma t)^2 + \ldots + \frac{1}{(N-1)!}(\Gamma t)^{N-1}\right\}$$

Note that the solutions for the initial level and for those intermediate levels $P_i(t)$ in the range $0 < i < N$ occur as products of two factors: a decaying exponential and coefficients from a Taylor expansion for a rising exponential. The solution for the band edge level population $P_0(t)$ is the product of a decaying exponential and a truncated Taylor expansion for a rising exponential. It follows from these solutions that the band edge state population is negligible until the time $t < [(N-1)!]^{1-N}/\Gamma$; thereafter, it rises to $P_0 = 1$.

An inspection of the solutions shows that as $t \to 0$, $P_N > P_{i\neq N}$, while as $t \to \infty$, $P_0 > P_{i>0}$. Therefore, the intermediate levels $0 < i < N$ are negligible and play an auxuliary role. This conclusion justifies the reduction of the model to initial and final states only. Since we are interested in reproducing general features from experimental spectroscopy, we focus on a narrow spectral window with a homogeneous density of electronic states, so that $E_i = i\varepsilon$, where $\varepsilon$ represents the energy difference between nearest electronic states. Within this model the expectation value of the energy of excitation and the relevant rate of the energy decrement read

$$\langle E\rangle = \varepsilon \sum_i iP_i \quad \text{and} \quad \frac{d\langle E\rangle}{dt} = \varepsilon \sum_i i\dot{P}_i \tag{14}$$

Using the equation of motion for $P_i$ and assuming that the total population of the band normalizes as $\Sigma_{i=0}^{\infty}P_i = 1$, the expression for the time derivative, $d\langle E\rangle/dt$, can be written as

$$\frac{1}{\Gamma\varepsilon}\frac{d\langle E\rangle}{dt} = -\sum_{i=1}^{N} P_i\{P_0 + \sum_{i=1}^{N} P_i\}^{-1} = -(1 - P_0(t))$$

Suppose that the initial excitation is at orbital $N$, so the expectation value of the energy starts at $\langle E\rangle(0) = N\varepsilon$. The energy decrement at the initial time equals $d\langle E\rangle/dt(0) = -\Gamma\varepsilon(1 - P_0(0))$. The ratio of the two yields normalized relaxation rates in the limits $t = 0$ and $t = \infty$:

$$\lim_{t\to 0}\left(\frac{d\langle E\rangle/dt}{\langle E\rangle}\right)_{t\to 0} = -\Gamma/N,$$
$$\lim_{t\to \infty}\left(\frac{d\langle E\rangle/dt}{\langle E\rangle}\right)_{t\to \infty} = 0 \tag{15}$$

These apply for equidistant levels with the rate of relaxation between neighboring levels represented by $\Gamma$. At time zero, all populations are concentrated in level $N$. This can be compared with the two-level system in which the rate of relaxation is $\Gamma'$, the energy difference is given by $E_1 - E_0 = \varepsilon'$, and the Pauli master equation is $\dot{P}_1 = \dot{P}_0 = -\Gamma P_1$. For such a model the rate of energy loss is

$$\left(\frac{d\langle E\rangle/dt}{\langle E\rangle}\right)_{t\to 0} = -\Gamma$$

Comparing these expressions for the $N$-level and two-level models, we conclude that, in a sequential process, the overall relaxation time is proportional to the number of levels that occur between the initial and final states. Therefore, to mimic a sequential process of $N$ steps using a simple two-level system, we must introduce the effective transfer rate for the two-level system, scaled by $N$, the number of intermediate levels: $\Gamma_{2\text{-levels}} = N\Gamma_{N\text{-levels}}$. This is the transformation we seek between $N$-level and two-level model parameters.

This comparison of relaxation rates can be extended to the comparison of exciton-phonon couplings. Generally, a relaxation $\Gamma$ originates from interactions with the bath $H_{SB} \sim J(Q)|i\rangle\langle j|$. The rate of wavefunction increment is $\dot{\psi} = -i\hbar H_{SB}\psi$, while the rate of population increment, which follows from the Fermi golden rule, is proportional to $|\langle H_{SB}\rangle|^2$. In our treatment, $J(Q) \approx J_0 + J'\cdot Q$, where $J_0 = 0$, since the system is close to equilibrium and transitions between states are adiabatic. Assuming $\Gamma \sim |\langle H_{SB}\rangle|^2 \sim |J'\cdot Q|^2$ and requiring $\Gamma_{2-\text{levels}} = N\Gamma_{N-\text{levels}}$, we obtain the following scaling,

$$|J'_{2\text{-levels}}| = \sqrt{N}|J'_{N\text{-levels}}|$$

For example, consider an initial excitation at level number 20, where the effective adiabatic coupling between two neighboring levels is about 2−3 meV. Then, in our approximate treatment using the effective two-level system, the NA coupling gains a factor of $(20)^{1/2} = 4.472$, which corresponds to 8.944−13.416 meV.

## ■ ACKNOWLEDGMENT

D.K. acknowledges the support by South Dakota Governor's Office of Economic Development and NSF award EPS0903804. Computational effort was supported by DOE, BES-Chemical Sciences, and NERSC Contract No. DE-AC02-05CH11231, allocation Award 84577 "Computational Modeling of Photocatalysis and Photoinduced Charge Transfer Dynamics on Surfaces". S.K. and D.K. are grateful to Kiril Tsemekhman for fruitful discussions. S.K. is grateful to Andrei Piryatinski for feedback on ideas. S.K. and D.K. thank Sergei Tretiak for hosting the visit at the Los Alamos National Lab during preparation of the manuscript. D.K. thanks V. Albert for discussions and editorial suggestions, the QTP at the University of Florida, and Prof. David Micha for a supportive research atmosphere, discussions, and hospitality. O.V.P. acknowledges NSF support, Grant CHE-1050405, for methods development and DOE support, Grant DE-FG02-05ER15755, for the quantum dot studies.

## ■ REFERENCES

(1) Klimov, V. I. *Semiconductor and Metal Nanocrystals: Synthesis and Electronic and Optical Properties*; Marcel Dekker: New York, 2004.
(2) Nozik, A. J. *Annu. Rev. Phys. Chem.* **2001**, *52*, 193–231.
(3) Murphy, J. E.; Beard, M. C.; Norman, A. G.; Ahrenkiel, S. P.; Johnson, J. C.; Yu, P.; Mii, O. I.; Ellingson, R. J.; Nozik, A. J. *J. Am. Chem. Soc.* **2006**, *128*, 3241–3247.
(4) Schaller, R. D.; Klimov, V. I. *Phys. Rev. Lett.* **2004**, *92*, 186601–4.

(5) Schaller, R. D.; Agranovich, V. M.; Klimov, V. I. *Nat. Phys.* **2005**, *1*, 189–194.
(6) Coe, S.; Woo, W. K.; Bawendi, M.; Bulovic, V. *Nature* **2002**, *420*, 800–803.
(7) Talapin, D. V.; Murray, C. B. *Science* **2005**, *310*, 86–89.
(8) Klimov, V. I. *J. Phys. Chem. B* **2000**, *104*, 6112–6123.
(9) Klimov, V. I.; Mikhailovsky, A. A.; McBranch, D. W.; Leatherdale, C. A.; Bawendi, M. G. *Phys. Rev. B* **2000**, *61*, R13349–R13352.
(10) Gorman, J.; Hasko, D. G.; Williams, D. A. *Phys. Rev. Lett.* **2005**, *95*, 090502–4.
(11) Petta, J. R.; Johnson, A. C.; Taylor, J. M.; Laird, E. A.; Yacoby, A.; Lukin, M. D.; Marcus, C. M.; Hanson, M. P.; Gossard, A. C. *Science* **2005**, *309*, 2180–2184.
(12) Dahan, M.; Levi, S.; Luccardini, C.; Rostaing, P.; Riveau, B.; Triller, A. *Science* **2003**, *302*, 442–445.
(13) Ellingson, R. J.; Blackburn, J. L.; Yu, P.; Rumbles, G.; Micic, O. I.; Nozik, A. J. *J. Phys. Chem. B* **2002**, *106*, 7758–7765.
(14) Schaller, R. D.; Sykora, M.; Pietryga, J. M.; Klimov, V. I. *Nano Lett.* **2006**, *6*, 424–429.
(15) Crooker, S. A.; Hollingsworth, J. A.; Tretiak, S.; Klimov, V. I. *Phys. Rev. Lett.* **2002**, *89*, 186802–4.
(16) Harbold, J. M.; Du, H.; Krauss, T. D.; Cho, K.-S.; Murray, C. B.; Wise, F. W. *Phys. Rev. B* **2005**, *72*, 195312–6.
(17) Califano, M.; Zunger, A.; Franceschetti, A. *Nano Lett.* **2004**, *4*, 525–531.
(18) Semenov, Y. G.; Kim, K. W. *Phys. Rev. Lett.* **2004**, *92*, 026601–4.
(19) Muljarov, E. A.; Takagahara, T.; Zimmermann, R. *Phys. Rev. Lett.* **2005**, *95*, 177405–4.
(20) Kamisaka, H.; Kilina, S. V.; Yamashita, K.; Prezhdo, O. V. *Nano Lett.* **2006**, *6*, 2295–2300.
(21) Prezhdo, O. V.; Rossky, P. J. *Phys. Rev. Lett.* **1998**, *81*, 5294–5297.
(22) Kilina, S. V.; Craig, C. F.; Kilin, D. S.; Prezhdo, O. V. *J. Phys. Chem. C* **2007**, *111*, 4871–4878.
(23) Cooney, R. R.; Sewall, S. L.; Anderson, K. E. H.; Dias, E. A.; Kambhampati, P. *Phys. Rev. Lett.* **2007**, *98*, 177403–4.
(24) Harbold, J. M.; Du, H.; Krauss, T. D.; Cho, K.-S.; Murray, C. B.; Wise, F. W. *Phys. Rev. B* **2005**, *72*, 195312.
(25) Kilina, S.; Kilin, D.; Prezhdo, O. *ACS Nano* **2009**, *3*, 93–99.
(26) Ellingson, R. J.; Beard, M. C.; Johnson, J. C.; Yu, P.; Micic, O. I.; Nozik, A. J.; Shabaev, A.; Efros, A. L. *Nano Lett.* **2005**, *5*, 865–871.
(27) Efros, A. L.; Kharchenko, V. A.; Rosen, M. *Solid State Commun.* **1995**, *93*, 281–284.
(28) Guyot-Sionnest, P.; Wehrenberg, B.; Yu, D. *J. Chem. Phys.* **2005**, *123*, 074709–7.
(29) Inerbaev, T. M.; Masunov, A. E.; Khondaker, S. I.; Dobrinescu, A.; Plamada, A.-V.; Kawazoe, Y. *J. Chem. Phys.* **2009**, *131*, 044106–6.
(30) Cooney, R. R.; Sewall, S. L.; Dias, E. A.; Sagar, D. M.; Anderson, K. E. H.; Kambhampati, P. *Phys. Rev. B* **2007**, *75*, 245311–14.
(31) Wise, F. W. *Acc. Chem. Res.* **2000**, *33*, 773–780.
(32) Ridley, B. K. *Quantum Process in Semiconducors*; Clarendon Press: Oxford, 1982.
(33) Ledebo, L. A.; Ridley, B. K. *J. Phys. C* **1982**, *15*, L961–L964.
(34) Schaller, R. D.; Pietryga, J. M.; Goupalov, S. V.; Petruska, M. A.; Ivanov, S. A.; Klimov, V. I. *Phys. Rev. Lett.* **2005**, *95*, 196401–4.
(35) Craig, C. F.; Duncan, W. R.; Prezhdo, O. V. *Phys. Rev. Lett.* **2005**, *95*, 163001–4.
(36) Habenicht, B. F.; Craig, C. F.; Prezhdo, O. V. *Phys. Rev. Lett.* **2006**, *96*, 187401–4.
(37) Fischer, S. R.; Habenicht, B. F.; Madrid, A. B.; Dunkan, W. R.; Prezhdo, O. V. *J. Chem. Phys.* **2011**, *134*, 024102–9.
(38) Tully, J. C. *J. Chem. Phys.* **1990**, *93*, 1061–1071.
(39) Hammes-Schiffer, S.; Tully, J. C. *J. Chem. Phys.* **1994**, *101*, 4657–4667.
(40) Parandekar, P. V.; Tully, J. C. *J. Chem. Phys.* **2005**, *122*, 094102–6.
(41) Marques, M. A. L.; Gross, E. K. U. *Annu. Rev. Phys. Chem.* **2004**, *55*, 427–455.
(42) Baer, R.; Neuhauser, D. *Phys. Rev. Lett.* **2005**, *94*, 043002–4.
(43) Li, X. S.; Tully, J. C.; Schlegel, H. B.; Frisch, M. J. *J. Chem. Phys.* **2006**, *123*, 084106–6.
(44) Coker, D. F. In *Computer Simulations in Chemical Physics*; Allen, M. P., Tildesley, D. J., Eds.; Kluwer Academic Publishers: Netherlands, 1993; pp 315−377.
(45) Murray, C. B.; Norris, D. J.; Bawendi, M. G. *J. Am. Chem. Soc.* **1993**, *115*, 8706–8715.
(46) Madelung, O. *Semiconductors, Data Handbook*, 3rd ed.; Springer: New York, 2004.
(47) Kilin, D.; Pereverzev, Y. V.; Prezhdo, O. V. *J. Chem. Phys.* **2004**, *120*, 11209–11223.
(48) Kilin, D.; Schreiber, M. *J. Lumin.* **2000**, *92*, 13–25.
(49) Franceschetti, A. *Phys. Rev. B* **2008**, *78*, 075418–6.
(50) Kondov, I.; Kleinekathofer, U.; Schreiber, M. *J. Chem. Phys.* **2003**, *119*, 6635–6646.
(51) Luis, A. *Phys. Rev. A* **2003**, *67*, 062113–4.
(52) Kresse, G.; Furthmüller, J. *Phys. Rev. B* **1996**, *54*, 11169–11186.
(53) Kresse, G.; Hafner, J. *Phys. Rev. B* **1994**, *49*, 14251–14269.
(54) Vanderbilt, D. *Phys. Rev. B* **1990**, *41*, 7892–7895.
(55) Perdew, J. P. *Electronic Structure of Solids*; Ziesche, P., Eschrig, H., Eds.; Akademie Verlag: Berlin, 1991.
(56) May, V.; Kühn, O. In *Charge and Energy Transfer Dynamics in Molecular Systems*; Wiley-VCH: Berlin, 2000; Chapter 3.
(57) Kilin, D. S.; Prezhdo, O. V.; Schreiber, M. *J. Phys. Chem. A* **2007**, *111*, 10212–10219.
(58) Kilin, D.; Kleinekathöfer, U.; Schreiber, M. *J. Phys. Chem. A* **2000**, *104*, 5413–5421.
(59) Kilin, D. S.; Micha, D. A. *Chem. Phys. Lett.* **2008**, *461*, 266–270.
(60) Kilin, D. S.; Micha, D. A. *J. Phys. Chem. Lett.* **2010**, *1*, 1073–1077.
(61) van Strien, A. J.; Schmidt, J.; Silbey, R. *Mol. Phys.* **1982**, *46*, 151–160.